*Nano Research* 2013, 6(1): 38–46
DOI 10.1007/s12274-012-0279-1
Research Article

ISSN 1998-0124
CN 11-5974/O4

# Composite of sulfur impregnated in porous hollow carbon spheres as the cathode of Li–S batteries with high performance

Kai Zhang, Qing Zhao, Zhanliang Tao, and Jun Chen (✉)

*Key Laboratory of Advanced Energy Materials Chemistry (Ministry of Education), Chemistry College, Nankai University, Tianjin 300071, China*

**Received:** 14 October 2012
**Revised:** 13 November 2012
**Accepted:** 14 November 2012



**KEYWORDS**

porous hollow carbon spheres,
mesopous/microporous multi-scale,
carbon–sulfur composite cathode,
Li–S batteries

## ABSTRACT

Carbon–sulfur composites as the cathode of rechargeable Li–S batteries have shown outstanding electrochemical performance for high power devices. Here, we report the promising electrochemical charge–discharge properties of a carbon–sulfur composite, in which sulfur is impregnated in porous hollow carbon spheres (PHCSs) via a melt-diffusion method. Instrumental analysis shows that the PHCSs, which were prepared by a facile template strategy, are characterized by high specific surface area (1520 $m^2 \cdot g^{-1}$), large pore volume (2.61 $cm^3 \cdot g^{-1}$), broad pore size distribution from micropores to mesopores, and high electronic conductivity (2.22 $S \cdot cm^{-1}$). The carbon–sulfur composite with a sulfur content of 50.2 wt.% displays an initial discharge capacity of 1450 $mA \cdot h \cdot g^{-1}$ (which is 86.6% of the theoretical specific capacity) and a reversible discharge capacity of 1357 $mA \cdot h \cdot g^{-1}$ after 50 cycles at 0.05 C charge–discharge rate. At a higher rate of 0.5 C, the capacity stabilized at around 800 $mA \cdot h \cdot g^{-1}$ after 30 cycles. The results illustrate that the porous carbon–sulfur composites with hierarchically porous structure have potential application as the cathode of Li–S batteries because of their effective improvement of the electronic conductivity, the repression of the volume expansion, and the reduction of the shuttling loss.

## 1 Introduction

Among various types of rechargeable batteries, Li–S batteries have attracted increasing attention due to their high theoretical specific capacity (1675 $mA \cdot h \cdot g^{-1}$) and energy density (2600 $W \cdot h \cdot kg^{-1}$) [1–7], which are several times greater than those of common lithium-ion batteries [8, 9]. In addition, Li–S batteries have great potential applications in high-energy-density devices because sulfur is abundant and low-cost [10]. However, the development of Li–S batteries has encountered the following difficulties. First, sulfur is electrically insulating, leading to a poor electronic conductivity ($5 \times 10^{-30}$ $S \cdot cm^{-1}$ at 25 ℃), a low utilization of the active

Address correspondence to chenabc@nankai.edu.cn

material, and a poor high-rate capability [11]. Second, the electrochemical reactions of sulfur with lithium ions occur step-by-step during the continuous charge-discharge processes, and the intermediate long-chain polysulfides are very soluble in conventional organic electrolytes. Furthermore, the dissolved polysulfides migrate to the Li anode, and then react with Li to form shorter chain polysulfides, which results in serious anode corrosion and a rapid increase of the internal resistance [12]. This "shuttle" phenomenon causes poor cycling ability and low coulombic efficiency. Third, volume expansion of sulfur is large during charge–discharge cycling, accelerating the capacity decline [13]. Therefore, it has been suggested that the combination of enhancing the electronic conductivity of the cathode, limiting the dissolution of polysulfides in the organic electrolyte, and repressing the volume expansion of sulfur are the main factors which will lead to an improved performance of Li–S batteries. To achieve these aims, different strategies have been attempted such as fabricating carbon–sulfur composites [14], preparing composite electrodes with conductive polymers [15], and optimizing the organic electrolyte [16]. Of these, carbon–sulfur composites have been considered as one of the most promising cathode materials for Li–S batteries because of their good electrochemical properties.

Recently, various types of carbon–sulfur composites have been fabricated. Compared with other carbon materials such as graphene [17], nanotubes [18], and nanofibers [19], porous carbon materials can strongly absorb polysulfides and buffer the volume expansion, leading to improved cycle life and coulombic efficiency. Moreover, porous carbon materials can be prepared in a simple, effective, and scalable way. Nazar's group [3] reported that nanostructured polymer-modified mesoporous carbon–sulfur composites showed an initial discharge capacity of 1320 $mA{\cdot}h{\cdot}g^{-1}$ and a discharge capacity of about 1100 $mA{\cdot}h{\cdot}g^{-1}$ after 10 cycles at a current density of 168 $mA{\cdot}g^{-1}$ (corresponding to 0.1C discharge rate). Cui's group [4] developed a facile method for preparing hollow carbon nanofiber–sulfur composites, showing an initial discharge capacity of 1560 $mA{\cdot}h{\cdot}g^{-1}$ and a reversible capacity of around 730 $mA{\cdot}h{\cdot}g^{-1}$ after 150 cycles at 0.2 C. Archer and co-workers [14] synthesized mesoporous hollow carbon sphere–sulfur composites, which displayed a reversible capacity of about 850 $mA{\cdot}h{\cdot}g^{-1}$ after 100 cycles at a discharge rate of 0.5 C. Wei et al. [20] found that mesopores can enhance the initial discharge capacity of carbon–sulfur composites due to the high specific surface areas, and micropores can effectively restrain the shuttling loss leading to improved cycle life. Therefore, the effect of pore size distribution and specific surface area of carbon–sulfur composites on the electrochemical properties of the materials are worth studying.

Here, we report a composite of sulfur impregnated in porous hollow carbon spheres (PHCSs) for use as the cathode of Li–S batteries with ultrahigh performance. The PHCSs were prepared through a facile self-assembly method and showed a broader pore size distribution (from micropores to mesopores) with hierarchically porous structure and a higher degree of graphitization than in a previous report [14]. The carbon–sulfur composites were synthesized via a melt-diffusion strategy. The weight ratio of sulfur to carbon was optimized and the carbon–sulfur composite with 50.2 wt.% sulfur showed the best electrochemical properties. At 0.05 C rate, the carbon–sulfur composites showed an ultrahigh discharge capacity of 1450 $mAh{\cdot}g^{-1}$ and a durable cycle life.

## 1 Experimental

### 1.1 Sample preparation

The PHCSs were synthesized by a facile template strategy. First, 0.5 g of phenolic resin was added to 20 mL of absolute ethanol and completely dissolved at 50 ℃. After that, 2 mL of tetraethylorthosilicate (TEOS) was added and the mixture stirred for 15 min to form a light yellow transparent solution. Second, a mixture of 10 mL of concentrated aqueous ammonia and 40 mL of ethanol was quickly added to the solution which was stirred for 3 h at 50 ℃. The obtained slurry was evaporated for 12 h at 60 ℃ and then the dried solid was thermally treated for 2 h at different calcination temperature (650, 750, and 850 ℃) under argon gas flow in a tube furnace. Finally, the black solid was washed with 10 wt.% HF solution to remove the silica and repeatedly centrifuged with distilled water until

the pH of the washings reached ~7. The black product was dried at 80 ℃ to obtain PHCSs.

The carbon–sulfur composites were fabricated via a melt-diffusion method. The PHCSs and the sulfur were mixed and then heated to 155 ℃ in a sealed vessel under an argon atmosphere with the heating rate of 5 ℃·min$^{-1}$. After 10 h, the carbon–sulfur composites were obtained.

### 1.2 Materials characterization

The structure and morphology of PHCSs and carbon–sulfur composites were characterized by powder X-ray diffraction (XRD, Rigaku MiniFlex600, Cu K$\alpha$ radiation) in the 2$\theta$ range 10°–80°, field-emission scanning electron microscopy (SEM, FEI Nanosem 430, 10 kV), and transmission electron microscopy (TEM, Philips Tecnai FEI, 200 kV). The Brunauer–Emmett–Teller (BET) specific surface area was analyzed by measuring the $N_2$ adsorption–desorption isotherm at 77 K on a BELSORP-mini instrument. Raman spectra were collected using a confocal Raman microscope (DXR, Thermo Fisher Scientific) with excitation at 532 nm from an argon-ion laser. The electronic conductivity of the as-prepared PHCSs was tested by a four-probe meter detector (RTS-8, China) at room temperature. The PHCSs were pressed into a wafer with 12 mm diameter and their thickness was measured using a spiral micrometer. Four metal probes with equal intervals were pressed on the surface of the PHCSs and the current passed through the two outer probes. The electronic conductivity was determined by measuring the potential between the two inner probes. The weight ratio of sulfur in the carbon–sulfur composite was measured using a Sulfur–Nitrogen Determination Apparatus (RPP-3000SN).

### 1.3 Electrochemical measurements

Electrochemical tests were performed with CR2032 coin-type cells. The cathodes were prepared from a mixture of the porous hollow carbon sphere–sulfur composites, carbon nanofibers, acetylene black, and polyvinylidene fluoride (PVDF) in *N*-methyl-2-pyrrolidone, with a weight ratio of 80:5:5:10. The obtained slurry was uniformly pasted onto aluminum foil, and dried at 80 ℃ for 12 h in vacuum. Lithium metal was used as the anode and reference electrode. The electrolyte was 1.0 M lithium bis(trifluoromethanesulfonyl)imide (LiTFSI) in a mixture of 1,3-dioxolane (DOL) and 1,2-dimethoxyethane (DME) (1:1, *v*/*v*). The coin cells were assembled in an argon-filled glove box (Mikrouna Universal 2440/750). Galvanostatic charge-discharge tests were performed in the range 1.5–3.0 V at different rates by using a LAND-CT2001A battery-testing instrument. Cyclic voltammograms (CVs) were recorded at a scan rate of 0.1 mV·s$^{-1}$ in the range 1.0–3.0 V on Parstat 263A potentiostat/galvanostat workstation (Princeton Applied Research & AMETEK Company). The electrochemical measurements were all conducted at room temperature.

## 2 Results and discussions

### 2.1 Characterization of the as-synthesized PHCSs and carbon–sulfur composites

The XRD patterns of PHCSs prepared at different calcination temperatures (650 ℃, 750 ℃, and 850 ℃) are shown in Fig. 1(a). The XRD patterns exhibit two broad diffraction peaks located at about 22.0° and 44.0° which can be indexed to (002) and (100) planes, respectively. The strong peak at 22.0° indicates the presence of partially graphitized structures in the PHCSs and the weak peak at 44.0° represents the quasi-amorphous frameworks [20]. Figure 1(b) shows the Raman spectra of the PHCSs obtained at different synthesis temperatures. Two peaks are observed at around 1590 and 1350 cm$^{-1}$. The peak at 1590 cm$^{-1}$ (G band) is assigned to the Raman active $E_{2g}$ mode of the graphitic carbon lattice vibration and the peak at 1350 cm$^{-1}$ (D band) corresponds to the $A_{1g}$ mode of disordered carbon, which is considered to originate from some kind of imperfection [21]. The intensity ratio of the D band to G band ($I_D/I_G$) is used to evaluate the graphitization degree of the carbon materials. As the synthesis temperature was increased from 650 to 850 ℃, the $I_D/I_G$ ratio of PHCSs decreased, which indicates that the sample prepared at 850 ℃ has the highest degree of graphitization and the best electronic conductivity [22]. An sp$^2$-hybridized carbon species has a strong chemical interaction with sulfur [23], leading to strong adsorption capability. The PHCSs

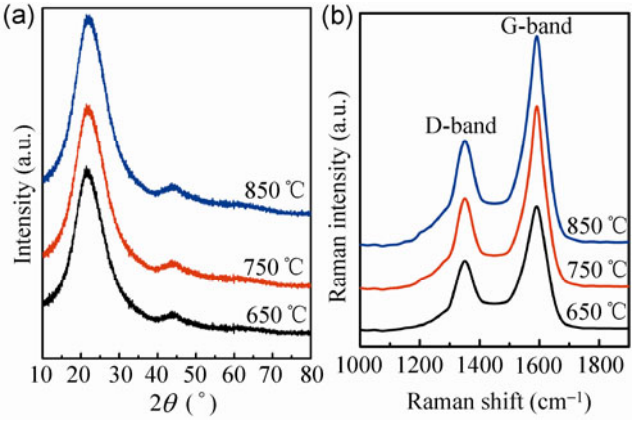


**Figure 1** XRD patterns (a) and Raman spectra (b) of the PHCSs prepared at different calcination temperatures (650 ℃ (black), 750 ℃ (red), and 850 ℃ (blue)).

were also analyzed by a four probe meter detector to measure their electronic conductivities. Detailed data are summarized in Table 1. The electronic conductivities of PHCSs heated at 650 ℃, 750 ℃, and 850 ℃ are 1.47, 2.08, and 2.22 S·cm$^{-1}$, respectively, consistent with their Raman spectra. The PHCSs prepared at 850 ℃ exhibit higher electronic conductivity, and so the sulfur was impregnated in this sample.

The SEM and TEM images of the PHCSs prepared at 850 ℃ are shown in Fig. 2. From Fig. 2(a), it can be seen that the carbon spheres have a highly uniform spherical shape with an average diameter of 100 nm. The corresponding TEM image in Fig. 2(b) shows that the carbon spheres have a hollow structure with a wrinkled shell and thin walls. Figure 2(c) depicts the $N_2$ adsorption/desorption isotherm of PHCSs prepared at 850 ℃. The curve exhibits the characteristics of both type Ⅰ and Ⅳ isotherms according to the IUPAC classification, which indicates the presence of a broad pore size ranging from micropores to mesopores. The BET specific surface area and total pore volume were

**Table 1** Detailed data for the four probe measurements

| PHCSs | Diameter (mm) | Thickness (mm) | Current (μA) | Electrical resistivity (Ω·cm) | Electronic conductivity (S·cm$^{-1}$) |
|---|---|---|---|---|---|
| PHCS-650 ℃ | 12 | 0.137 | 0.569 | 0.68 | 1.47 |
| PHCS-750 ℃ | 12 | 0.140 | 0.581 | 0.48 | 2.08 |
| PHCS-850 ℃ | 12 | 0.125 | 0.518 | 0.45 | 2.22 |

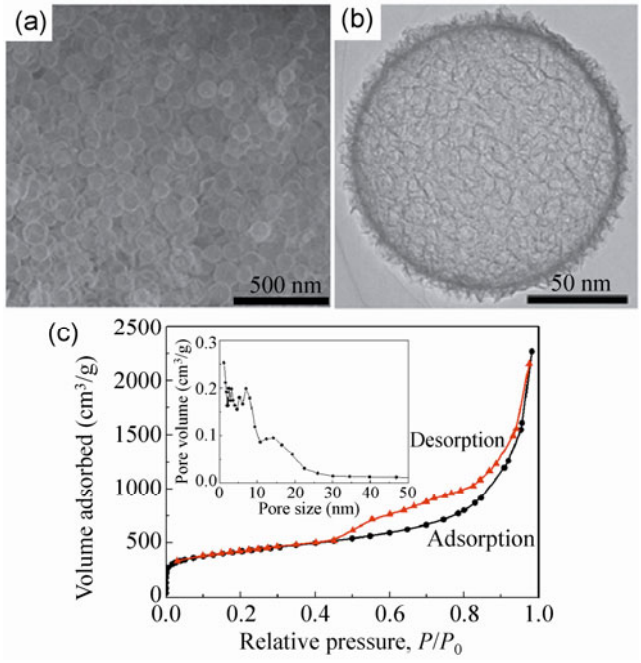


**Figure 2** SEM (a) and TEM (b) images of PHCSs prepared at 850 ℃ and its $N_2$ adsorption/desorption isotherm (c) measured at 77 K with the corresponding pore size distribution (insert figure).

1520 m$^2$·g$^{-1}$ and 2.61 cm$^3$·g$^{-1}$, respectively. It is suggested that these hollow carbon spheres with large pore volume and high surface area can strongly adsorb polysulfides, minimizing the dissolution of polysulfides in the organic electrolyte. The pore sizes (see the insert in Fig. 2(c)) are mainly in the range 1 to 25 nm, consistent with the adsorption/desorption isotherms. The average pore diameter of PHCSs is 7.15 nm, and the pores whose diameters are between 1 and 8 nm possess larger pore volume than the other pores. During the sulfur deposition process, the multi-scale porous structure facilitates diffusion of molten sulfur and sulfur gas adsorption, making sulfur exist in a highly dispersed state and avoiding aggregation of the sulfur.

The sublimed sulfur was impregnated in the PHCSs prepared at 850 ℃ through a melt-diffusion strategy to fabricate carbon–sulfur composites. Figure 3 shows the XRD patterns of the PHCSs, sublimed sulfur, and carbon–sulfur composites with different sulfur contents. The sharp diffraction peaks in the XRD spectrum of sublimed sulfur illustrate its crystalline state. As the sulfur content increases, the XRD curves of the carbon–sulfur composites change obviously. The sharp diffraction peaks of sulfur disappear entirely when

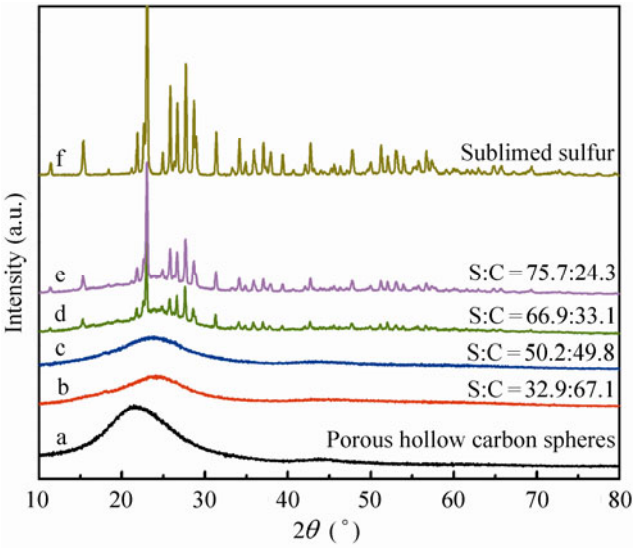


**Figure 3** XRD patterns of the PHCSs (a), sublimed sulfur (f), and carbon–sulfur composites with different contents of sulfur (b)–(e).

the weight ratio of sulfur to carbon is smaller than 1:1, which indicates that sulfur is highly dispersed in the pores of hollow carbon spheres [19]. However, when the sulfur content exceeds 66.9 wt.%, the appearance of many sharp peaks confirms that a portion of sulfur is not impregnated into the pores but covers the surface of the hollow carbon spheres, leading to poor cycling performance. The broad peaks of amorphous carbon are barely obvious in the carbon–sulfur composite with 75.7 wt.% sulfur, indicating that sulfur completely covers the surface of the hollow carbon spheres. Based on the XRD results, the carbon–sulfur composite with 50.2 wt.% sulfur was used as the active material to fabricate Li–S batteries.

The textural properties of PHCSs and carbon–sulfur composites are listed in Table 2. The BET surface area and pore volume decrease as the content of sulfur increases, denoting that the sulfur is infused in the pores of the hollow carbon spheres. When the sulfur content is higher than 66.9 wt.%, the BET surface area and pore volume change only slightly, suggesting that the pores are fully filled and the excess sulfur can only cover the surface of the hollow carbon spheres. The maximum value of sulfur impregnated in the pores can be calculated as follows [3]:

$$m_s = V_p \times \rho_{Li_2S} \times M_s / M_{Li_2S} \quad (1)$$

where $m_s$, $V_p$, $\rho_{Li_2S}$, $M_s$, and $M_{Li_2S}$ are the maximum mass of sulfur impregnated in the pores per gram of carbon, pore volume of PHCSs (2.61 $cm^3 \cdot g^{-1}$), density of $Li_2S$ (1.66 $g \cdot cm^{-3}$), and molar masses of sulfur (32 $g \cdot mol^{-1}$) and $Li_2S$ (46 $g \cdot mol^{-1}$), respectively. According to the calculation, a maximum of 3.01 g of sulfur is infused into the pores of 1.00 g of hollow carbon spheres. After depositing excess sulfur, the intermediate lithium polysulfides escape from the pores, resulting in poor cycling performance. Therefore, a suitable sulfur content is important in order to achieve high load and good electrochemical properties. Compared with the other samples, the composite with 50.2 wt.% sulfur has both high load and appropriate residual pore volume to provide a transport pathway for $Li^+$ ions, ensure infiltration of the organic electrolyte, and accommodate the volume expansion during cycling [3].

Figure 4 shows the SEM, TEM, and HRTEM images of the carbon–sulfur composite with 50.2 wt.% sulfur. After sulfur particles were deposited in the pores of PHCSs, the morphology of the carbon spheres barely changed (Fig. 4(a)). The magnified SEM image in Fig. 4(b) shows that the carbon–sulfur composite has a hollow structure with shell thickness of ~10 nm. The wrinkled shell is composed of many nanoplates, which interweave to form an open porous structure. The interior hollow space can accommodate volume expansion during the discharge, and the porous structure provides a large interface area between the composite electrode and the electrolyte [14]. During the charge-discharge processes, the pores can restrain dissolution of the polysulfides and minimize the shuttling loss. The thin shells reduce the path length

**Table 2** BET specific surface areas and pore volumes of PHCSs and carbon–sulfur composites.

| Material | | BET surface area ($m^2 \cdot g^{-1}$) | Pore volume ($cm^3 \cdot g^{-1}$) |
|---|---|---|---|
| PHCSs | | 1520 | 2.6103 |
| Carbon–sulfur composites | S:C = 32.9:67.1 | 157.9 | 0.2507 |
| | S:C = 50.2:49.8 | 89.7 | 0.1135 |
| | S:C = 66.9:33.1 | 39.2 | 0.0087 |
| | S:C = 75.7:24.3 | 22.7 | 0.0023 |

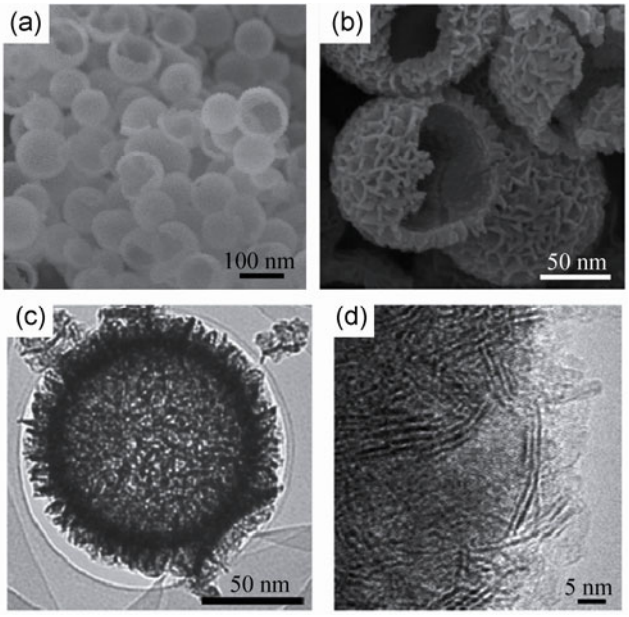


**Figure 4** SEM (a), (b), TEM (c), and high-resolution TEM (HRTEM) (d) images of carbon–sulfur composites with 50.2 wt.% sulfur.

for carrier transport in the composite materials, which enhances their kinetic properties. Figure 4(c) shows a TEM image of a typical porous hollow carbon sphere–sulfur composite, and illustrates that the majority of the pores are filled with sulfur nanoparticles. The HRTEM image in Fig. 4(d) shows that the shells have abundant porous channels which are beneficial for the fast transport of $Li^+$ ions.

### 2.2 Electrochemical measurements

Electrochemical measurements on the carbon–sulfur composites were carried out using coin cells prepared following similar procedures to those in our previous reports [24, 25]. The electrolyte was 1.0 M LiTFSI in a mixture of DOL and DME (1:1, *v*/*v*). Typical discharge and charge curves of the carbon–sulfur composites with different sulfur contents at 0.05 C rate are shown in Fig. 5. As expected, two discharge plateaus are observed at 2.30 and 2.05 V, which can be assigned to the two-step reaction of $S_8$. There are two corresponding charge plateaus at about 2.25 and 2.45 V, indicating the oxidation of $Li_2S$. In the examined range, the carbon–sulfur composite with a sulfur content of 32.9 wt.% showed the highest discharge capacity of 1457 mA·h·g$^{-1}$, while the composite with a sulfur

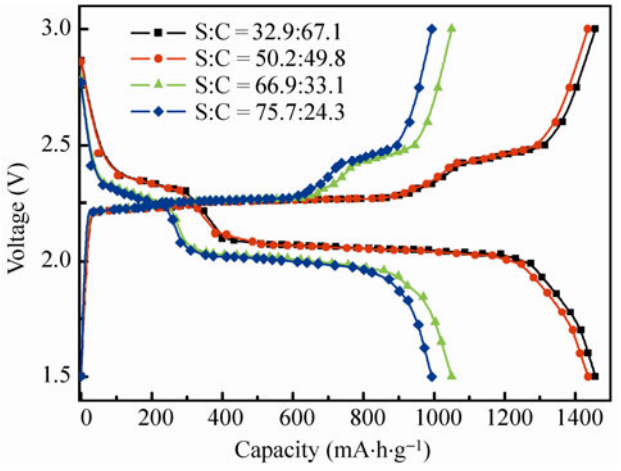


**Figure 5** Typical discharge and charge curves of the carbon–sulfur composites with different sulfur contents at 0.05 C rate between 1.5 and 3.0 V.

content of 50.2 wt.% displayed a high discharge capacity of 1436 mA·h·g$^{-1}$. Further increasing the sulfur content to 66.9 wt.% decreased the capacity due to the reduced pore volume which blocks the electrolyte infiltration and $Li^+$ ion transport. Therefore, the sample with 50.2 wt.% sulfur has the optimal sulfur content.

Figure 6 shows typical CV measurements for the carbon–sulfur composite with 50.2 wt.% sulfur at the first, fifth, and tenth cycles. At the first cycle, two obvious reduction peaks are located at 2.32 and 1.92 V, which can be attributed to the reduction of the $S_8$ ring to higher-order lithium polysulfides, and the reduction of higher-order lithium polysulfides to

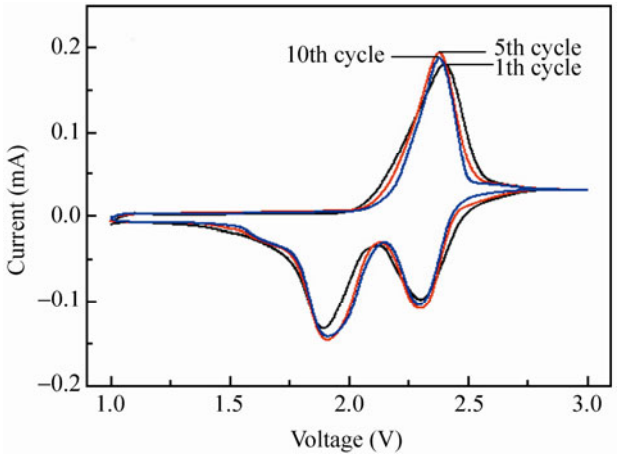


**Figure 6** Typical cyclic voltammograms of the carbon–sulfur composite with 50.2 wt.% sulfur at a scan rate 0.1 mV·s$^{-1}$ between 1.0 V and 3.0 V.

lower-order lithium polysulfides or $Li_2S$, respectively [12, 26]. These two changes correspond to the two discharge plateaus in the discharge curve. The two expected oxidation peaks overlap because of the high potential polarization between lithium polysulfides and the insoluble lithium sulfide [27]. However, only one oxidation peak is observed at about 2.42 V, indicating the oxidation process of $Li_2S$. The CV measurements illustrate that the cathode materials have excellent electrochemical reversibility due to the porous hollow structure and good electronic conductivity of the carbon–sulfur composite.

In order to investigate the cycling performance and rate capability of the carbon–sulfur composite with 50.2 wt.% sulfur, galvanostatic discharge and charge cycling was performed between 1.5 and 3.0 V. Figure 7(a) depicts the first cycle discharge and charge curves of the composite cathode at different rates. The first discharge capacity at 0.05 C is 1450 mA·h·g$^{-1}$ which is 86.6% of the theoretical specific capacity. The high initial capacity results from the unique microporous/mesoporous conductive structure with multichannels for ion transportation. With the increase of the discharge rate from 0.05 to 0.5 C, the first discharge capacity slightly fades, but almost no overcharge is observed, indicating that the shuttling loss has been minimized. The coulombic efficiencies are all above 98%, illustrating that the multi-scale porous structures have a great potential for giving enhanced discharge–charge properties. The cycling performance of carbon–sulfur composites at different discharge rates is shown in Fig. 7(b). The 1st and 50th discharge capacities at discharge rates of 0.05, 0.1, 0.2, and 0.5 C are summarized in Table 3. An ultrahigh reversible capacity of 1357 mA·h·g$^{-1}$ is obtained at 0.05 C after 50 cycles, showing a capacity decay of 6.4%. The microporous/mesoporous channels ensure immersion of the electrolyte, serving as a favorable $Li^+$ ion path for electrolyte penetration and allowing for fast ionic transport [28]. Furthermore, the microporous/mesoporous multi-scale structure strongly adsorbs polysulfides thus suppressing the shuttling loss, and accommodating the volume expansion of sulfur. Thus, it shows an excellent capacity retention, which can be exploited in high-energy-density devices. At a higher rate of 0.1 C, excellent initial discharge capacity and

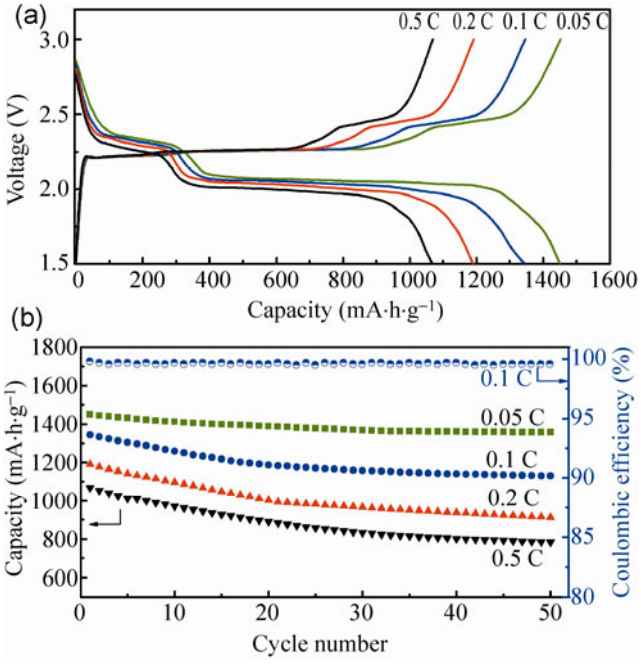


**Figure 7** (a) Typical discharge and charge curves of the carbon–sulfur composite with 50.2 wt.% sulfur at different discharge rates between 1.5 V and 3.0 V, and (b) cycling performance of carbon–sulfur composite at different discharge rates.

**Table 3** The discharge capacities at the 1st ($C_1$) and the 50th ($C_{50}$) cycle as well as the capacity ratio of $C_1$ to $C_{50}$ for carbon–sulfur composite cathodes at discharge rates of 0.05 C, 0.1 C, 0.2 C, and 0.5 C

| | 0.05 C | 0.1 C | 0.2 C | 0.5 C |
|---|---|---|---|---|
| $C_1$ (mA·h·g$^{-1}$) | 1450 | 1345 | 1190 | 1068 |
| $C_{50}$ (mA·h·g$^{-1}$) | 1357 | 1130 | 912 | 784 |
| $C_{50}/C_1$ | 93.6% | 84.0% | 76.6% | 73.4% |

ideal cycling performance are also achieved. The first discharge capacity is 1345 mA·h·g$^{-1}$ and the reversible capacity remains about 1130 mA·h·g$^{-1}$ after 50 cycles, retaining a high coulombic efficiency of 99.6%. In addition, for a high current density of 837.5 mA·g$^{-1}$ (0.5 C), the capacity stabilized at around 800 mA·h·g$^{-1}$ after 30 cycles, and slight decay is observed for the next 20 cycles. This can be attributed to the high electronic conductivity and multi-scale porous structure of the carbon matrix. As expected, the carbon–sulfur composite with 50.2 wt.% sulfur shows a durable cycling capability and high rate performance.

On the basis of the above results, the ideal initial discharge capacity, durable cycling capability and high rate performance can be understood in terms of the structure of the carbon–sulfur composite (Fig. 8) having

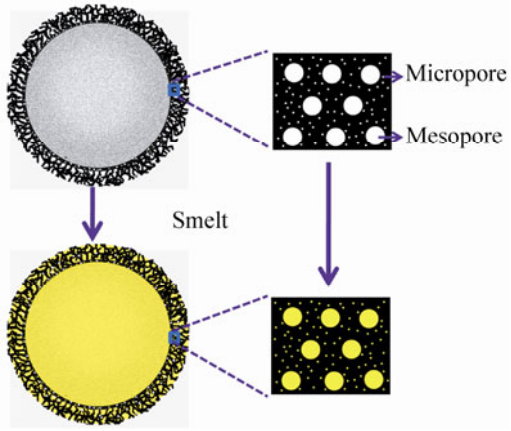


**Figure 8** Schematic illustrations of PHCSs and the carbon–sulfur composite.

the following characteristics. First, the PHCSs have high graphitization degree, and the $sp^2$-hybridized carbon has a strong chemical interaction with sulfur [14, 23]. In addition, the as-prepared PHCSs show high electronic conductivity of 2.22 $S \cdot cm^{-1}$, which improves the electron transport of the carbon–sulfur composite. Furthermore, the porous structure is advantageous for sulfur adsorption during the melt-diffusion preparation, which results in sulfur existing in a highly dispersed state [29]. Second, the hierarchical porous structure considerably reduces the dissolution of polysulfides and thus minimizes the shuttling loss. It is suggested that the mesopores enable the carbon–sulfur composite to have a high initial discharge capacity, and the micropores improve the cycle life [20]. Third, the electrochemical reactions of the sulfur cathode during charge–discharge cycles are combined with a series of electronic and phase transitions, which make the sulfur electrode expand during discharging and shrink when charging [13, 30]. The large pore volume and hollow structure provide enough space to accommodate the volume expansion of the sulfur. Therefore, the hollow carbon sphere–sulfur composites with multi-scale porous structures have potential application as cathode materials in Li–S batteries with high performance.

## 3 Conclusions

We have fabricated porous hollow carbon spheres with large pore volume and high electronic conductivity through a facile template method. The carbon–sulfur composites were synthesized by a melt-diffusion strategy, and the optimal weight ratio of sulfur to carbon is 50.2:49.8 for use as a cathode material. The composites effectively improve the electronic conductivity, inhibit the dissolution of polysulfides, and accommodate the volume expansion of sulfur, so the Li–S batteries display a high performance. The first discharge capacity of the carbon–sulfur composite with a sulfur content of 50.2 wt.% is 1450 $mA \cdot h \cdot g^{-1}$ at 0.05 C, which is 86.6% of the theoretical specific capacity. After 50 cycles, the capacity remains as high as 1357 $mA \cdot h \cdot g^{-1}$, a capacity fading of only 6.4%. At a higher rate of 0.5 C, the capacity stabilizes at around 800 $mA \cdot h \cdot g^{-1}$ after 30 cycles. Consequently, the hollow carbon sphere–sulfur composites with hierarchical porous structure have great potential for application in high-energy-density Li–S batteries.

## Acknowledgment

This work was supported by the National 973 Program (No. 2011CB935900), the National Nature Science Foundation of China (No. 21076108), the National 111 project of China's Higher Eduction (No. B12015), and the Fundamental Research Funds for the Central Universities.

## References

[1] Kim, J.; Lee, D. J.; Jung, H. G.; Sun, Y. K.; Hassoun, J.; Scrosati, B. An advanced lithium–sulfur battery. *Adv. Funct. Mater.*, in press, DOI: 10.1002/adfm.201200689.

[2] Bruce, P. G.; Freunberger, S. A.; Hardwick, L. J.; Tarascon, J. M. Li–$O_2$ and Li–S batteries with high energy storage. *Nat. Mater.* **2012**, *11*, 19–29.

[3] Ji, X.; Lee, K. T.; Nazar, L. F. A highly ordered nanostructured carbon–sulphur cathode for lithium–sulphur batteries. *Nat. Mater.* **2009**, *8*, 500–506.

[4] Zheng, G.; Yang, Y.; Cha, J. J.; Hong, S. S.; Cui, Y. Hollow carbon nanofiber-encapsulated sulfur cathodes for high specific capacity rechargeable lithium batteries. *Nano Lett.* **2011**, *11*, 4462–4467.

[5] Sun, H.; Xu, G.-L.; Xu, Y.-F.; Sun, S.-G.; Zhang, X.; Qiu, Y.; Yang, S. A composite material of uniformly dispersed sulfur on reduced graphene oxide: Aqueous one-pot synthesis, characterization and excellent performance as the cathode

in rechargeable lithium-sulfur batteries. *Nano Res.* **2012**, *5*, 726–738.

[6] Wang, J.-Z.; Lu, L.; Choucair, M.; Stride, J. A.; Xu, X.; Liu, H. K. Sulfur–graphene composite for rechargeable lithium batteries. *J. Power Sources* **2011**, *196*, 7030–7034.

[7] Yang, Y.; Yu, G.; Cha, J. J.; Wu, H.; Vosgueritchian, M.; Yao, Y.; Bao, Z.; Cui, Y. Improving the performance of lithium–sulfur batteries by conductive polymer coating. *ACS Nano* **2011**, *5*, 9187–9193.

[8] Xiao, X.; Lu, J.; Li, Y. $LiMn_2O_4$ microspheres: Synthesis, characterization and use as a cathode in lithium ion batteries. *Nano Res.* **2010**, *3*, 733–737.

[9] Cheng, F.; Liang, J.; Tao, Z.; Chen, J. Functional materials for rechargeable batteries. *Adv. Mater.* **2011**, *23*, 1695–1715.

[10] Liang, C.; Dudney, N. J.; Howe, J. Y. Hierarchically structured sulfur/carbon nanocomposite material for high-energy lithium battery. *Chem. Mater.* **2009**, *21*, 4724–4730.

[11] Fu, Y.; Manthiram, A. Core–shell structured sulfur–polypyrrole composite cathodes for lithium–sulfur batteries. *RSC Adv.* **2012**, *2*, 5927–5929.

[12] Ji, L.; Rao, M.; Aloni, S.; Wang, L.; Cairns, E. J.; Zhang, Y. Porous carbon nanofiber–sulfur composite electrodes for lithium/sulfur cells. *Energy Environ. Sci.* **2011**, *4*, 5053–5059.

[13] He, X.; Ren, J.; Wang, L.; Pu, W.; Jiang, C.; Wan, C. Expansion and shrinkage of the sulfur composite electrode in rechargeable lithium batteries. *J. Power Sources* **2009**, *190*, 154–156.

[14] Jayaprakash, N.; Shen, J.; Moganty, S. S.; Corona, A.; Archer, L. A. Porous hollow carbon@sulfur composites for high-power lithium–sulfur batteries. *Angew. Chem. Int. Ed.* **2011**, *50*, 5904–5908.

[15] Wu, F.; Chen, J.; Chen, R.; Wu, S.; Li, L.; Chen, S.; Zhao, T. Sulfur/polythiophene with a core/shell structure: Synthesis and electrochemical properties of the cathode for rechargeable lithium batteries. *J. Phys. Chem. C* **2011**, *115*, 6057–6063.

[16] Lin, Z.; Liu, Z.; Fu, W.; Dudney, N. J.; Liang, C. Phosphorous pentasulfide as a novel additive for high-performance lithium–sulfur batteries. *Adv. Funct. Mater.* **2012**, DOI: 10.1002/adfm.201200696.

[17] Wang, H.; Yang, Y.; Liang, Y.; Robinson, J. T.; Li, Y.; Jackson, A.; Cui, Y.; Dai, H. Graphene-wrapped sulfur particles as a rechargeable lithium–sulfur battery cathode material with high capacity and cycling stability. *Nano Lett.* **2011**, *11*, 2644–2647.

[18] Guo, J.; Xu, Y.; Wang, C. Sulfur–impregnated disordered carbon nanotubes cathode for lithium–sulfur batteries. *Nano Lett.* **2011**, *11*, 4288–4294.

[19] Elazari, R.; Salitra, G.; Garsuch, A.; Panchenko, A.; Aurbach, D. Sulfur-impregnated activated carbon fiber cloth as a binder-free cathode for rechargeable Li–S batteries. *Adv. Mater.* **2011**, *23*, 5641–5644.

[20] Wei, S.; Zhang, H.; Huang, Y.; Wang, W.; Xia, Y.; Yu, Z. Pig bone derived hierarchical porous carbon and its enhanced cycling performance of lithium–sulfur batteries. *Energy Environ. Sci.* **2011**, *4*, 736–740.

[21] Evers, S.; Nazar, L. F. Graphene-enveloped sulfur in a one pot reaction: A cathode with good coulombic efficiency and high practical sulfur content. *Chem. Commun.* **2012**, *48*, 1233–1235.

[22] Ferrari, A. C.; Robertson, J. Interpretation of Raman spectra of disordered and amorphous carbon. *Phys. Rev. B* **2000**, *61*, 14095–14107.

[23] Ji, L.; Rao, M.; Zheng, H.; Zhang, L.; Li, Y.; Duan, W.; Guo, J.; Cairns, E. J.; Zhang, Y. Graphene oxide as a sulfur immobilizer in high performance lithium/sulfur Cells. *J. Am. Chem. Soc.* **2011**, *133*, 18522–18525.

[24] Zhang, X.; Cheng, F.; Zhang, K.; Liang, Y.; Yang, S.; Liang, J.; Chen, J. Facile polymer-assisted synthesis of $LiNi_{0.5}Mn_{1.5}O_4$ with a hierarchical micro–nano structure and high rate capability. *RSC Adv.* **2012**, *2*, 5669–5675.

[25] Li, C.; Zhang, S.; Cheng, F.; Ji, W.; Chen, J. Porous $LiFePO_4$/NiP composite nanospheres as the cathode materials in rechargeable lithium-ion batteries. *Nano Res.* **2008**, *1*, 242–248.

[26] Li, X.; Cao, Y.; Qi, W.; Saraf, L. V.; Xiao, J.; Nie, Z.; Mietek, J.; Zhang, J. G.; Schwenzer, B.; Liu, J. Optimization of mesoporous carbon structures for lithium–sulfur battery applications. *J. Mater. Chem.* **2011**, *21*, 16603–16610.

[27] Cao, Y.; Li, X.; Aksay, I. A.; Lemmon, J.; Nie, Z.; Yang, Z.; Liu, J. Sandwich-type functionalized graphene sheet–sulfur nanocomposite for rechargeable lithium batteries. *Phys. Chem. Chem. Phys.* **2011**, *13*, 7660–7665.

[28] Cheng, F.; Wang, H.; Zhu, Z.; Wang, Y.; Zhang, T.; Tao, Z.; Chen, J. Porous $LiMn_2O_4$ nanorods with durable high-rate capability for rechargeable Li-ion batteries. *Energy Environ. Sci.* **2011**, *4*, 3668–3675.

[29] Li, N.; Zheng, M.; Lu, H.; Hu, Z.; Shen, C.; Chang, X.; Ji, G.; Cao, J.; Shi, Y. High-rate lithium–sulfur batteries promoted by reduced graphene oxide coating. *Chem. Commun.* **2012**, *48*, 4106–4108.

[30] Yuan, L.; Yuan, H.; Qiu, X.; Chen, L.; Zhu, W. Improvement of cycle property of sulfur-coated multi-walled carbon nanotubes composite cathode for lithium/sulfur batteries. *J. Power Sources* **2009**, *189*, 1141–1146.